Deep inelastic neutron scattering from orthorhombic ordered HCl: Short-time proton dynamics and anomalous neutron cross sections

R. Senesi*
Istituto Nazionale per la Fisica della Materia, Consiglio Nazionale delle Ricerche, UdR Tor Vergata, Via della Ricerca Scientifica 1, 00133, Roma, Italy

D. Colognesi
Istituto dei Sistemi Complessi, Consiglio Nazionale delle Ricerche, Via Madonna del Piano s.n.c., 50019 Sesto Fiorentino (FI), Italy

A. Pietropaolo
Istituto Nazionale per la Fisica della Materia, Consiglio Nazionale delle Ricerche, UdR Tor Vergata and Dipartimento di Fisica, Università degli Studi di Roma—Tor Vergata, Via della Ricerca Scientifica 1, 00133, Roma, Italy

T. Abdul-Redah
Physics Laboratory, University of Kent at Canterbury, Canterbury, Kent CT2 7NR, United Kingdom
(Received 3 March 2005; revised manuscript received 10 May 2005; published 16 August 2005)

Deep inelastic neutron scattering measurements from orthorhombic ordered HCl are presented and analyzed in order to clarify the problem of an anomalous deficit in the neutron-proton cross section found in previous experiments on various materials. A reliable model for the HCl short-time single-particle dynamics, including atomic vibrational anisotropies and deviations from the impulsive approximation, is set up. The model HCl response function is transformed into simulated time-of-flight spectra, taking carefully into account the effects of instrumental resolution and the filter absorption profile used for neutron energy analysis. Finally, the experimental values of the anomalous reduction factor for the neutron-proton cross section are extracted by comparing simulated and experimental data. Results show a 34% reduction of the H cross section, varying with the scattering angle in a range centered at 53°. In addition, the same approximate procedure used in earlier studies is also employed, providing results in reasonable agreement with the more rigorous ones, and confirming the substantial reliability of the past work on this subject.

DOI: 10.1103/PhysRevB.72.054119 PACS number(s): 61.12.Ex, 61.80.Hg, 63.20.Dj

I. INTRODUCTION

Deep inelastic neutron scattering (DINS) is a unique technique[1] providing useful information on the short-time dynamics of nuclei in various condensed matter systems, similarly to the more traditional x-ray Compton scattering from electrons. From an early stage in the 1960s, where DINS could only measure the single-particle mean kinetic energy in weakly bound systems [e.g., liquid and superfluid ^{4}He (Refs. 2–5)], this technique has undergone a remarkable development since the middle 1980s when intense fluxes of hot and epithermal neutrons were made available from spallation pulsed neutron sources like IPNS (Argonne National Laboratory, USA), KENS (KEK, Japan) and ISIS (Rutherford Appleton Laboratory, U.K.). Nowadays it is possible to extract details about the single-particle momentum distribution in liquid and superfluid helium,[6] solid helium,[7] and liquid neon,[8] making use of high-resolution chopper spectrometers, while, through filter-difference instruments exploiting epithermal neutrons, the free-recoil regime implied by DINS has been largely extended, so much to include nuclei in strongly bound molecular systems, such as dihydrogen,[9] graphite,[10] water,[11] hydrogen sulfide,[12] zirconium hydride,[13] lithium hydride,[14] and various others. Finally, in some special cases, even a reconstruction of the Born-Oppenheimer effective potential felt by the scattering particle has been successfully accomplished.[15]

However, the continuous exploration of always wider regions of energy and momentum transfers revealed unexpected and puzzling features in the short-time dynamics of light nuclei: in 1997 Chatzidimitriou-Dreismann *et al.* presented DINS measurements on liquid H_2O and on its mixtures with D_2O, reporting large anomalies in the behavior of the H and D neutron scattering cross sections (bound) as a function of the hydrogen-deuterium concentration ratio.[16] Practically, the ratios between the areas of the recoil peaks of H and D were extracted for the various mixtures and a peculiar deficit in the signal scattered from protons was observed, as their total cross section (bound) was lower than the accepted value:[17] $\sigma_H = 82.03 \times 10^{-28}$ m^2. Two years later a second kind of cross-section anomaly was discovered by Karlsson *et al.*[18] in DINS measurements on NbH_x and NbH_xD_y: the ratio between the areas of the recoil peaks of H and Nb was found to be lower than expected and strongly dependent on the scattering angle, while the analogous quantity with D replacing H shows only small deviations from standard neutron scattering theory.[19] Finally, in the last four years, similar anomalies were observed in several DINS experiments on other fully protonated and partially deuterated solid and liquid systems (benzene,[20] polystyrene,[21] formvar,[22] palladium hydride,[23] liquid hydrogen and deuterium,[24] lithium hydride,[25] etc.), exhibiting sometimes waterlike behavior (i.e., severely "missing" protons but no

relevant angular dependence), sometimes an NbH-like one [i.e., H cross section (bound) lower than expected and strongly angle dependent]. The aforementioned measurements were performed using a unique experimental apparatus: the eVS epithermal neutron spectrometer[26] and, after 2001, its successor Vesuvio,[27] both inverse-geometry resonant-filter instruments installed at the ISIS pulsed neutron source. Given the extreme range of momentum and energy transfers explored by this neutron instrument where the energy transfer dependence of scattering cross sections can be measured up to approximately 50 eV (see Sec. II for details), the independent tests usually performed through other kinds of neutron spectrometers were practically impossible. After the publication of the measured DINS anomalies, some aspects of the eVS-Vesuvio data analysis procedure were criticized, mainly insisting on three points: (1) the so-called convolution approximation, which is routinely employed to account for the instrumental resolution;[28] (2) the general use of a simplified neutron absorption profile for gold and uranium resonant filters;[29] (3) the numerical stability of the Jacobian supposedly used for transforming measured data from the time-of-flight (TOF) domain to the energy transfer one.[30] These criticisms triggered a lively debate on the whole data reduction procedure in the case of inverse-geometry resonant-filter spectrometers, which was thoroughly tested either using analytical calculations,[31] or comparing experimental eVS data with numerical Monte Carlo simulations.[32] Unfortunately these two approaches yielded opposite conclusions, since the latter work[32] claimed to have proved that (1), (2) the approximate treatment of neutron absorption profile and instrumental resolution, both important in the evaluation of the atomic mean kinetic energy, plays a negligible role as far as the intensity deficit is concerned; (3) the Jacobian expression is irrelevant since experimental data are directly analyzed in the time-of-flight domain. In addition, this scientific debate quickly branched into a series of additional discussions on similar (or opposite) results obtained through other neutron techniques (neutron interferometry[33] and epithermal neutron transmission[34]), and even other probes (Raman,[35] inelastic x-ray,[36] and electron-nucleus[22] scattering). Unfortunately no final consensus has been reached so far on the reliability of the anomalous DINS cross-section measurements, and this is exactly one of the reasons that stimulated the experiments presented here.

The purpose of this work is to clarify the problem of the anomalous neutron-scattering cross-section in DINS through measurements performed on a simply structured molecular crystal containing protons in an electronic environment rather different from that of metal hydrides. To this aim solid fully ordered hydrogen chloride (in short phase-III HCl) has been selected, following the motivations listed below: (1) the simplicity of the molecule (diatomic) and the lattice structure (face-centered orthorhombic, two molecules per primitive unit cell, space group $Cmc2_1$);[37] (2) the conspicuous polar character of the molecule, which, at least in the gas phase, implies an effective hydrogen charge of $+0.178e$;[38] (3) a reasonable knowledge of the phase-III HCl lattice dynamics, both at the Γ point (i.e., at zero momentum transfer) and in the whole first Brillouin zone, via Raman and ir spectroscopies,[39,40] incoherent inelastic neutron scattering,[41,42] and various lattice dynamics simulations,[43–47] the last of which managed to accurately reproduce even fine details like the correct magnitude of the Davydov splitting.[48] Finally, it is worth noting that hydrogen halides (HF, HCl, HBr, and HI) constitute in themselves an interesting class of compounds, despite their simple diatomic molecular structure.[49] For instance, HCl and HBr are the simplest known molecular ferroelectric materials.[50] They exhibit both a very strong long-range dipole-dipole interaction and a significant quadrupole-quadrupole one, which are probably responsible for the existence of several different crystal structures and for a quite high melting temperature. As an example, HCl shows a phase transition from III to II (orthorhombic, orientationally disordered, space group *Cmca*) at $T=98.4$ K, from II to I (cubic, orientationally disordered, space group $Fm\bar{3}m$) at $T=120.0$ K, and finally melts at $T=158.9$ K.[51] Most authors regard these interactions as a peculiar case of hydrogen bonding and some evidence for this kind of bonding has been still found even in the liquid phase.[52]

The rest of the paper will be organized as follows. The experimental DINS procedure will be described in detail in Sec. II, while Sec. III will be fully devoted to the setting up of a reliable model of the anisotropic response function describing deep inelastic neutron scattering from solid orthorhombic HCl. Section IV will deal with the neutron time-of-flight data analysis, both of experimental and simulated spectra, making use of two different procedures. In Sec. V, we will discuss the data analysis results and we will check the validity of the opposite approaches used in Refs. 28 and 29, and in Ref. 32, respectively. Finally, Sec. VI will contain the conclusions of the present study.

II. EXPERIMENT

The measurements were performed on the inverse-geometry electron-volt spectrometer VESUVIO, operating at the ISIS spallation pulsed neutron source, making use of an incident pulsed neutron beam with energies in the epithermal range 0.1–100 eV.[27] The scattered neutron energies were determined by the resonance filter difference technique:[53] in this method absorption ^{197}Au filters (two distinct thickness values were available) mounted on aluminium frames and placed between sample and detectors, are cycled in and out of the scattered neutron beam every 300 s in order to average out the drifts in detector efficiency during the single runs. Difference between the measurements, with the filter in the beam and with the filter out of the beam, provides the neutron counting rate absorbed by the foil and determines the energy of the scattered neutrons via standard TOF technique.[54] The resonance energy E_r and energy width (full width at half maximum), ΔE_r, of the ^{197}Au are known from the literature[53,55] to be $E_r=4906(2)$ meV, and $\Delta E_r=182(8)$ meV at room temperature. As for the VESUVIO detectors, the present measurements employed only the four forward-scattering banks, since no DINS from protons can be recorded in backscattering:[19] these four modules contained a total of 32 Li-glass scintillators placed on the equatorial plane and covering an angular range

$32.8° < \theta < 67.6°$, with θ being the scattering angle. This section of the VESUVIO spectrometer describes curved trajectories in the instrumental kinematic space, roughly limited by the following figures: $25 < Q < 200$ Å^{-1} and $-0.2 < \hbar\omega < 120$ eV, where $\hbar Q$ and $\hbar\omega$ are the momentum and energy transfers, respectively. Finally, the important question of the VESUVIO instrumental resolution will be dealt with in detail in Sec. IV.

DINS measurement was carried out on a single polycrystalline sample of HCl kept at a temperature $T=4.00(2)$ K in its orthorhombic ordered phase III. After collecting background data from the empty cryostat, we cooled down the empty sample container to the experimental temperature (i.e., $T=4.00$ K) and then we measured its TOF neutron spectrum up to an integrated proton current of 2379.7 μA h. The sample cell was made of aluminum (1.0-mm-thick walls) with a circular-slab geometry. The sample thickness was 1.5 mm and the cell diameter (50.0 mm) was larger than the neutron beam cross section (circular, umbra diameter 30.0 mm). The sample container was warmed up to $T=179.0$ K and hydrogen chloride (99%+ pure gas from CK Gas) was allowed to condense in it. The pressure of the gas handling system was set to $p=1.4$ bar [slightly larger than the corresponding saturated vapor pressure (SVP)] in order to make sure that the cell was completely filled with liquid [SVP is 0.58 bar at $T=179.0$ K (Ref. 56)]. Then we cooled down the cell back to $T=4.00$ K and the system pressure stabilized at $p=0.12$ bar. At this point we started recording the scattering spectrum up to an integrated proton current of 4778.1 μA h (roughly 26.5 h of beam time). The stability of the thermodynamic conditions during the experiment was quite satisfactory. Temperature fluctuations never exceeded $\Delta T=0.01$ K and pressure fluctuations were always smaller than $\Delta p=3$ mbar. The total temperature uncertainty (i.e. standard deviation) estimated for our measurements, $\sigma(T)=0.02$ K, was mainly due to a tiny gradient across the vertical dimension of the sample cell. Finally, it is worth noting that the polycrystalline nature of the sample measured was guaranteed by the fact that HCl was frozen in phase I (at $T=158.9$ K) and subsequently it underwent two disruptive phase transitions (i.e., from I to II at $T=120.0$ K, and from II to III at $T=98.4$ K) before reaching the thermodynamic conditions of the measurement (i.e., $T=4.00$ K).

III. MODEL ANISOTROPIC RESPONSE FUNCTION

As it will be made clearer in the next section, an accurate description of the DINS response function from phase-III HCl is crucial for the accomplishment of a refined TOF data analysis procedure able to cope with the criticisms[28,29] already mentioned in the introductory section of the present work. Let us start by recalling some basic features about DINS: as mentioned in Sec. II, in a measurement performed on VESUVIO the wave-vector transfer $\mathbf{Q}$ corresponding to recorded spectral features is approximately varying[27] between 25 and 200 Å^{-1}. In this kinematic range it is customary to make use of the well-known *incoherent approximation*,[57] since the spatial correlations between different atoms have been certainly canceled by the exceedingly low values of the Debye-Waller factors involved. Under this assumption, the neutron scattering double-differential cross section can be written as

$$\left(\frac{d^2\sigma}{d\Omega\, d\omega}\right)_{\mathrm{DINS}} = \frac{1}{4\pi}\sqrt{\frac{E_1}{E_0}}\sum_n x_n \sigma_n S_s^{(n)}(\mathbf{Q},\omega), \qquad (1)$$

where E_0 and E_1 are the incoming and outcoming neutron energies, respectively, x_n is the atomic concentration of the nonequivalent species n, σ_n is its total (i.e., coherent plus incoherent) neutron scattering cross section (bound), and, finally, $S_s^{(n)}(\mathbf{Q},\omega)$ is the self-inelastic-structure factor for the aforementioned species n. In other words, in the framework of the incoherent approximation the scattered signal can be expressed as a simple linear combination of the scattering from the various nonequivalent species, weighted by the respective total cross sections. It is worthwhile to note that the term *nonequivalent species* has been employed here instead of *isotopic species*, since the same isotope can exhibit different dynamical behaviors if located, for example, in nonequivalent molecular or crystallographic sites. So, as for orthorhombic ordered HCl, a remark has to be made: in spite of having two molecules per elementary unit cell, this crystal exhibits only one C_s symmetry site.[45] In this way the number of nonequivalent species becomes $n=3$, i.e., H, ^{35}Cl, and ^{37}Cl.

If the other kinematic variable of the VESUVIO measurements is now considered, that is the energy transfer $\hbar\omega$, one realizes that this quantity [roughly ranging between −0.2 and 120 eV (Ref. 27)] is in most of the cases exceedingly larger than all the vibrational frequencies observed in phase-III HCl [the highest being the B_2 H—Cl stretching at about 82.188 THz, corresponding to 0.339 90 eV (Ref. 45)]. Under this condition, the H and Cl nuclei hit by neutrons recoil almost freely, since the interaction time of the scattering event turns out to be much shorter than the atomic vibration period.[1] This is precisely the reason why the dynamics explored by DINS experiments is also named *short-time self-dynamics*. As far as the DINS spectra from HCl are concerned, the almost-free-recoil scenario just described manifests itself in the well-known *impulse approximation* (IA):[19] each $S_s^{(n)}(\mathbf{Q},\omega)$ assumes a simple functional form $S_{s,IA}^{(n)}(\mathbf{Q},\omega)$, which is directly related to the nth-nucleus momentum distribution along the direction of the wave-vector transfer $\hat{\mathbf{Q}}$, via the West scaling,

$$S_{s,IA}^{(n)}(\mathbf{Q},\omega) = \frac{M_n}{\hbar Q} J_n(y_n,\hat{\mathbf{Q}}), \qquad (2)$$

where M_n is the mass of the nth nucleus, $Q=|\mathbf{Q}|$, $\hbar^{-1}J_n(\hbar y_n,\hat{\mathbf{Q}})$ is the aforementioned one-dimensional momentum distribution along $\hat{\mathbf{Q}}$, and y_n stands for the West variable given by

$$y_n = \frac{M_n}{\hbar Q}\left(\omega - \frac{\hbar Q^2}{2M_n}\right). \qquad (3)$$

However, the asymptotic formula of Eq. (2) is in practice never attained, since the IA implies the unphysical double

limit $Q\to\infty, \omega\to\infty$, keeping y_n=const for any n. For this reason Eq. (2) is generally replaced by

$$S_s^{(n)}(\mathbf{Q},\omega)=\frac{M_n}{\hbar Q}F_n(y_n,\mathbf{Q}), \tag{4}$$

where $F_n(y_n,\mathbf{Q})$ retains an additional dependence on Q, irreducible to the simple West scaling. Such a dependence is generally known[1] as the *final-state effect* (FSE). Various methods for the approximate evaluation of the FSE have been devised so far,[58] the simplest and most widely used of which is surely the so-called *additive approach*.[58,59] It reads

$$F_n(y_n,\mathbf{Q})=\left(1+\sum_{p=3}^{\infty}(-1)^p A_p^{(n)}(\mathbf{Q})\frac{\partial^p}{\partial y_n^p}\right)J_n(y_n,\hat{\mathbf{Q}}), \tag{5}$$

where

$$A_3^{(n)}(\mathbf{Q})=\frac{M_n}{12\hbar^2 Q}\left\langle\sum_{j,k=1}^{3}\hat{Q}_j\frac{\partial^2 V}{\partial r_j^{(n)}\partial r_k^{(n)}}\hat{Q}_k\right\rangle_n,$$

$$A_4^{(n)}(\mathbf{Q})=\frac{M_n^2}{24\hbar^4 Q^2}\left\langle\left(\sum_{j=1}^{3}\hat{Q}_j\frac{\partial V}{\partial r_j^{(n)}}\right)^2\right\rangle_n, \tag{6}$$

with V being the potential energy of the system, and $\langle\ldots\rangle_n$ the quantum-statistical average including the sum over all the nuclei belonging to the nth species. In addition there exist rather complicated expressions for $A_5^{(n)}(\mathbf{Q})$ and $A_6^{(n)}(\mathbf{Q})$,[60] which contain leading terms in $1/Q$ and $1/Q^2$, respectively. However, as pointed out by Sears[58] and Rinat,[61] Eq. (5) shows a rather annoying inconvenience, since, differently from the much less amenable Gersch-Rodriguez-Smith approach,[62] there is no guarantee that $A_5^{(n)}(\mathbf{Q})$ and $A_6^{(n)}(\mathbf{Q})$ exhaust the $1/Q$ and $1/Q^2$ terms of the FSE, respectively. In other words, after any truncation of Eq. (5), it is impossible to evaluate how fast the approximate additive approach series converges to the IA as $Q\to\infty$.

An interesting exception to the aforementioned dim scenario is represented by a class of systems fulfilling the so-called *Gaussian approximation*,[63] i.e., where the time-Fourier transform of the self-inelastic-structure factor can be cast as

$$S_s^{(n)}(\mathbf{Q},\omega)=\frac{1}{2\pi}\int_{-\infty}^{\infty}\exp(-i\omega t)\exp\left(-\sum_{j,k}Q_j U_{jk}^{(n)}(t)Q_k\right)dt, \tag{7}$$

with $U_{jk}^{(n)}(t)$ being a time-dependent complex tensor. It is possible to show[64] that, provided $U_{jk}^{(n)}(t)$ is analytical in $t=0$ and its short-time limit is given by

$$\lim_{t\to 0}U_{jk}^{(n)}(t)=-\frac{i\hbar t}{2M_n}\delta_{jk}+O(t^2), \tag{8}$$

the Gaussian approximation implies the following form for the additive approach:

$$F_n(y_n,\mathbf{Q})=\left(1-A_3^{(n)}(\mathbf{Q})\frac{\partial^3}{\partial y_n^3}+A_4^{(n)}(\mathbf{Q})\frac{\partial^4}{\partial y_n^4}+\frac{[A_3^{(n)}(\mathbf{Q})]^2}{2}\frac{\partial^6}{\partial y_n^6}\right)J_n(y_n,\hat{\mathbf{Q}})+O(Q^{-3}), \tag{9}$$

where it is simple to verify that in this case all the $1/Q$ and $1/Q^2$ terms have been included in the sum. In addition, other important simplifications occur. The nth-nucleus momentum distribution along the direction of the wave-vector transfer $\hat{\mathbf{Q}}$ assumes a purely multivariate Gaussian functional form[12,65]

$$J_n(y_n,\hat{\mathbf{Q}})=\frac{1}{\sqrt{2\pi}\sigma_n(\hat{\mathbf{Q}})}\exp\left(-\frac{y_n^2}{2\sigma_n^2(\hat{\mathbf{Q}})}\right), \tag{10}$$

where $\sigma_n(\hat{\mathbf{Q}})$, together with $A_3^{(n)}(\mathbf{Q})$ and $A_4^{(n)}(\mathbf{Q})$, can be expressed as a function of the odd moments (and Bose-corrected even moments) of the atom-projected power spectrum of the velocity autocorrelation tensor $Z_{jk}^{(n)}(\omega)$, which is defined as[63]

$$Z_{jk}^{(n)}(\omega)=\frac{4M_n}{\pi\hbar\omega}\int_0^{\infty}\mathrm{Im}\langle v_j^{(n)}(0)v_k^{(n)}(t)\rangle\sin(\omega t)dt. \tag{11}$$

Thus, after some algebraic manipulations, one obtains

$$F_n(y_n,\mathbf{Q})\simeq\left(1+\frac{A_3^{(n)}(\mathbf{Q})}{[2\sigma_n^2(\hat{\mathbf{Q}})]^{3/2}}H_3\{y_n[2\sigma_n^2(\hat{\mathbf{Q}})]^{-1/2}\}+\frac{A_4^{(n)}(\mathbf{Q})}{[2\sigma_n^2(\hat{\mathbf{Q}})]^2}H_4\{y_n[2\sigma_n^2(\hat{\mathbf{Q}})]^{-1/2}\}+\frac{[A_3^{(n)}(\mathbf{Q})]^2}{2[2\sigma_n^2(\hat{\mathbf{Q}})]^3}H_6\{y_n[2\sigma_n^2(\hat{\mathbf{Q}})]^{-1/2}\}\right)J_n(y_n,\hat{\mathbf{Q}}), \tag{12}$$

where $H_m(\cdots)$ are mth-order Hermite polynomials, and[66]

$$\sigma_n^2(\hat{\mathbf{Q}})=\frac{M_n}{2\hbar}\sum_{j,k=1}^{3}\int_0^{\infty}\hat{Q}_j Z_{jk}^{(n)}(\omega)\hat{Q}_k\omega\coth\left(\frac{\hbar\omega}{2k_BT}\right)d\omega,$$

$$A_3^{(n)}(\mathbf{Q})=\frac{M_n^2}{12\hbar^2 Q}\sum_{j,k=1}^{3}\int_0^{\infty}\hat{Q}_j Z_{jk}^{(n)}(\omega)\hat{Q}_k\omega^2 d\omega,$$

$$A_4^{(n)}(\mathbf{Q})=\frac{M_n^3}{48\hbar^3 Q^2}\sum_{j,k=1}^{3}\int_0^{\infty}\hat{Q}_j Z_{jk}^{(n)}(\omega)\hat{Q}_k\omega^3\coth\left(\frac{\hbar\omega}{2k_BT}\right)d\omega. \tag{13}$$

The condensed matter systems where the Gaussian approximation can be safely applied include, of course, the ideal case of a perfectly harmonic crystalline lattice,[67] but it has been experimentally proved that a larger class of low-temperature solid systems (sometimes exhibiting non-negligible anharmonic effects due to the very light masses of their constituent atoms), such as solid hydrogen,[68] lithium hydride,[69] and ice[70] can be also dealt with within a reasonable accuracy in the framework of the Gaussian approxima-

tion. For this reason orthorhombic ordered HCl at $T=4$ K will be also described in what follows making use of this approximation, namely, via Eqs. (12) and (13).

The evaluation of $\sigma_n(\hat{\mathbf{Q}})$, $A_3^{(n)}(\mathbf{Q})$, and $A_4^{(n)}(\mathbf{Q})$ is then accomplished through Eqs. (13) starting from $Z_{jk}^{(n)}(\omega)$ which, in turn, can be estimated either via classical molecular dynamics, or via pseudoharmonic lattice dynamics. However the former method, which includes potential anharmonicity effects, is not recommendable at very low temperatures where the quantum nature of lattice vibrations becomes crucial. For this reason, a standard lattice dynamics code[71] (namely, GULP) in connection with the simple semiempirical potential scheme devised by Grout and Leech[43] is employed. In practice, one relies on the harmonic relationship[72] between the atom-projected power spectrum of the velocity autocorrelation tensor and the phonon frequencies $\omega(\mathbf{q},g)$ and polarization vectors $\mathbf{e}(n,\mathbf{q},g)$:

$$Z_{jk}^{(n)}(\omega)=\frac{1}{N}\sum_{g=1}^{12}\sum_{\mathbf{q}\in 1\mathrm{BZ}} e_j^*(n,\mathbf{q},g)e_k(n,\mathbf{q},g)\delta(\omega-\omega(\mathbf{q},g)), \tag{14}$$

where $\mathbf{q}$ is the phonon wave vector contained in the first Brillouin zone, N is the number of these wave vectors, and g is labeling the 12 phonon branches of phase-III HCl. Plugging Eq. (14) into Eqs. (13), one finally writes

$$\sigma_n^2(\hat{\mathbf{Q}})=\frac{M_n}{2\hbar N}\times\sum_{g=1}^{12}\sum_{\mathbf{q}\in 1\mathrm{BZ}}|\hat{\mathbf{Q}}\cdot\mathbf{e}(n,\mathbf{q},g)|^2\omega(\mathbf{q},g)\coth\left(\frac{\hbar\omega(\mathbf{q},g)}{2k_BT}\right),$$

$$A_3^{(n)}(\mathbf{Q})=\frac{M_n^2}{12\hbar^2QN}\sum_{g=1}^{12}\sum_{\mathbf{q}\in 1\mathrm{BZ}}|\hat{\mathbf{Q}}\cdot\mathbf{e}(n,\mathbf{q},g)|^2\omega(\mathbf{q},g)^2,$$

$$A_4^{(n)}(\mathbf{Q})=\frac{M_n^3}{48\hbar^3Q^2N}\times\sum_{g=1}^{12}\sum_{\mathbf{q}\in 1\mathrm{BZ}}|\hat{\mathbf{Q}}\cdot\mathbf{e}(n,\mathbf{q},g)|^2\omega(\mathbf{q},g)^3\coth\left(\frac{\hbar\omega(\mathbf{q},g)}{2k_BT}\right). \tag{15}$$

At this stage Eq. (12) can be evaluated making use of the $\omega(\mathbf{q},g)$ and $\mathbf{e}(n,\mathbf{q},g)$ derived from the GULP lattice dynamics simulation. However, in order to increase the accuracy of the calculation, the values of $\omega(\mathbf{q},g)$ derived from the Grout and Leech potential scheme are rescaled by a factor obtained from the ratio between experimental[39,40] and simulated[43] phonon frequencies at the Γ point, $\omega(\mathbf{q}=0,g)$. The choice of the $\mathbf{q}$ wave vectors contained in the first Brillouin zone is accomplished using the well-known Monkhorst-Pack method.[73] As for the chlorine isotopic distribution, considering the relative smallness of the mass difference, an approximate correction procedure is applied. Lattice dynamics simulations are executed fixing the Cl atomic mass to its natural mean value, $M_{\mathrm{Cl}}=35.453$ amu,[74] then $\sigma_n^2(\hat{\mathbf{Q}})$, $A_3^{(n)}(\mathbf{Q})$, and $A_4^{(n)}(\mathbf{Q})$ are simply scaled by the following constants: $(M_{\mathrm{Cl}}/M_n)^{1/2}$, M_{Cl}/M_n, and $(M_{\mathrm{Cl}}/M_n)^{3/2}$, respectively, where $M_n=34.969$ amu for ^{35}Cl and $M_n=36.966$ amu for ^{37}Cl.[74] Finally, given the polycrystalline nature of the HCl sample employed, an average over $\hat{\mathbf{Q}}$ is also used:

$$\langle F_n(y_n,\mathbf{Q})\rangle_\Omega=\frac{1}{4\pi}\int_\Omega \mathbf{F}_n(y_n,\mathbf{Q})d\hat{\mathbf{Q}}. \tag{16}$$

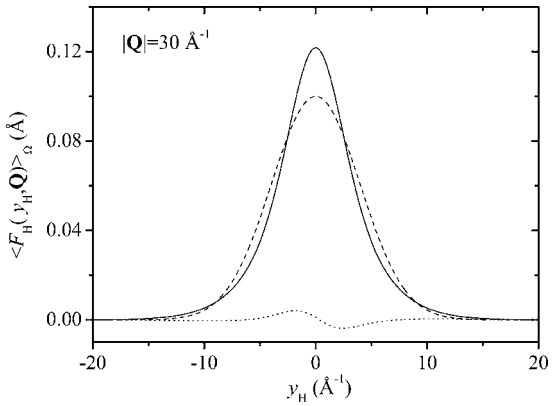

FIG. 1. $\hat{\mathbf{Q}}$-averaged asymptotic proton response function, $\langle J_{\mathrm{H}}(y_{\mathrm{H}},\hat{\mathbf{Q}})\rangle_\Omega$ (full line), together with the corresponding final state effect component $\langle F_{\mathrm{H}}(y_{\mathrm{H}},\mathbf{Q})-J_{\mathrm{H}}(y_{\mathrm{H}},\hat{\mathbf{Q}})\rangle_\Omega$ (dotted line), evaluated at $|\mathbf{Q}|=30$ Å^{-1}. In addition a fictitious purely Gaussian asymptotic response function (dashed line), exhibiting the same y variance as $\langle J_{\mathrm{H}}(y_{\mathrm{H}},\hat{\mathbf{Q}})\rangle_\Omega$, is shown for comparison.

An example of the present model of anisotropic DINS response function from orthorhombic ordered HCl is reported in Fig. 1, where the $\hat{\mathbf{Q}}$-averaged IA proton contribution $\langle J_{\mathrm{H}}(y_{\mathrm{H}},\hat{\mathbf{Q}})\rangle_\Omega$ is plotted together with the respective FSE components $\langle F_{\mathrm{H}}(y_{\mathrm{H}},\mathbf{Q})-J_{\mathrm{H}}(y_{\mathrm{H}},\hat{\mathbf{Q}})\rangle_\Omega$. Since an important feature of the described response function calculation is the exact treatment of the single-particle dynamics anisotropy, a fictitious purely Gaussian IA response function $J_{\mathrm{H}}(y_{\mathrm{H}})$, exhibiting the same y variance as $\langle J_{\mathrm{H}}(y_{\mathrm{H}},\hat{\mathbf{Q}})\rangle_\Omega$, is also shown as a comparison.

IV. TIME-OF-FLIGHT DATA ANALYSIS

The difference between filter-in and filter-out VESUVIO spectra yielded the experimental DINS time-of-flight profiles. An example of these raw TOF spectra $C(t,\langle\theta\rangle)$ (where $\langle\theta\rangle$ is the average scattering angle) for seven detectors is shown in Fig. 2. From this figure one can appreciate the change of the hydrogen recoil peak position as a function of the average scattering angle with respect to the three overlapping peaks due to ^{27}Al, ^{35}Cl, and ^{37}Cl. The scattering contributions given by the aluminum sample container were carefully subtracted, making use of the empty-cell measurements and taking accurately into account the neutron-energy variation of the HCl transmission power.[75] The multiple scattering counting rates were also estimated through a DINS-oriented Monte Carlo simulation routine[76] and found to be

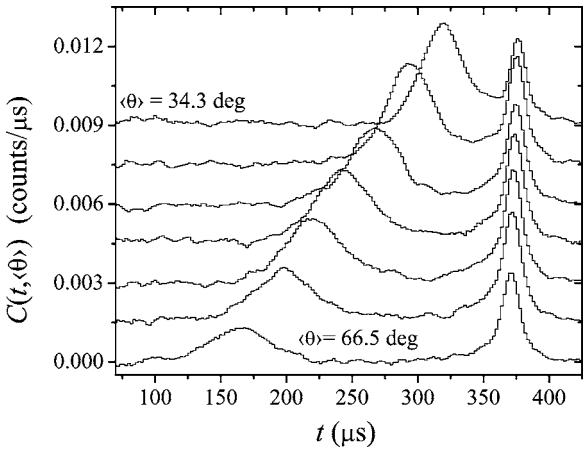

FIG. 2. Difference time-of-flight neutron spectra from orthorhombic ordered HCl at $T=4.00$ K, for seven detectors in the average scattering angle range $34.3° < \langle\theta\rangle < 66.5°$ (top to bottom). Left-side broad peak is caused by H, while right-side narrow peak by Cl plus Al from the container. Data have been smoothed for graphic reasons.

small, but not totally negligible (ranging from 8.1% to 12.2% of the total scattering in the TOF region $30 < t < 498$ μs). So these contributions were removed from the experimental TOF spectra, which finally were corrected for the HCl self-shielding attenuation.[75]

After performing all the appropriate corrections, the processed TOF spectra $C_1(t,\langle\theta\rangle)$ had to be related to the sample double-differential scattering cross section, and, as explained in Sec. II, to the proton and chlorine DINS response functions. Considering that Eq. (1) explicitly contains the total neutron scattering cross sections (bound) of H, ^{35}Cl, and ^{37}Cl, it was clear that once expressed $C_1(t,\langle\theta\rangle)$ in terms of $\langle F_n(y_n,\mathbf{Q})\rangle_\Omega$ with $n=\{\mathrm{H},{}^{35}\mathrm{Cl},{}^{37}\mathrm{Cl}\}$, σ_n were directly obtainable through a linear fitting procedure. As already mentioned in Sec. I, the relationship between VESUVIO time-of-flight spectra (single scattering) and sample double-differential cross sections has been deeply clarified and dealt with in detail in the last five years mainly owing to the problem of the anomalous proton cross sections. Thus one had just to report the VESUVIO time-of-flight equation following the most recent literature on the subject,[28,29,31,32]

$$
\begin{aligned}
C_1(t,\langle\theta\rangle) = {} & n_T \Delta\Omega \rho_s d_s \int_{-\infty}^{\infty} dt_0 \int_0^{\pi} d\theta \int_0^{\infty} dL_0 \\
& \times \int_0^{\infty} dL_1 P(t_0,\theta,L_0,L_1) \int_0^{\infty} dE_0 \Phi(E_0) \\
& \times \int_0^{\infty} dE_1 \eta(E_1)[1 - T_{\mathrm{Au}}(E_1)] \\
& \times \delta\left(t - t_0 - L_0\sqrt{\frac{m_n}{2E_0}} - L_1\sqrt{\frac{m_n}{2E_1}}\right) \\
& \times \left(\frac{d^2\sigma}{d\Omega\, d\hbar\omega}\right)_{\mathrm{DINS}},
\end{aligned}
\tag{17}
$$

where m_n is the neutron mass, n_T is the number of neutron pulses included in one phase of the measurement (say "foil in"), $\Delta\Omega$ is the solid angle defining the detector acceptance, while ρ_s and d_s are the sample molecular density and thickness, respectively. As for the other quantities, some comments are needed: $P(t_0,\theta,L_0,L_1)$ is the probability distribution that a given neutron quits the moderator with a time delay t_0, travels from the moderator to the sample along a flight path L_0, is scattered at an angle θ, and finally travels from the sample to the detector along a flight path L_1. Obviously a normalization condition applies:

$$
\int_{-\infty}^{\infty} dt_0 \int_0^{\pi} d\theta \int_0^{\infty} dL_0 \int_0^{\infty} dL_1 P(t_0,\theta,L_0,L_1) = 1. \tag{18}
$$

To any practical purpose, $P(t_0,\theta,L_0,L_1)$ is factorized assuming a reasonable lack of correlation between the various instrumental parameters t_0, θ, L_0, and L_1. So one ends with a product of distribution functions characterised by appropriate means (i.e., $\langle t_0\rangle$, $\langle\theta\rangle$, $\langle L_0\rangle$, and $\langle L_1\rangle$, known from the instrument calibration) and standard deviations

$$
\begin{aligned}
P(t_0,\theta,L_0,L_1) = {} & G(t_0 - \langle t_0\rangle) U(\theta - \langle\theta\rangle) G(L_0 - \langle L_0\rangle) G(L_1 \\
& - \langle L_1\rangle),
\end{aligned}
\tag{19}
$$

where $G(\cdots)$ and $U(\cdots)$ stand for Gaussian and uniform distributions, respectively. The function $\Phi(E_0)$ represents the energy distribution of the incoming neutron flux hitting the sample in a single pulse. In the case of instruments like VESUVIO, in the range of the epithermal neutrons $\Phi(E_0) \propto E_0^{-0.9}$.[32,54] As for the two E_1-dependent quantities, $\eta(E_1)$ stands for the Li-glass detector efficiency, and $T_{\mathrm{Au}}(E_1)$ is the Au filter transmission. Both functions can be written in the same exponential form, but while for the former a simple expression is normally used,

$$
\eta(E_1) = \exp(-D/\sqrt{E_1}), \tag{20}
$$

with D being a proper constant, the latter has to be described in detail as pointed out in Ref. 29:

$$
T_{\mathrm{Au}}(E_1) = \exp\{-\rho_f d_f[\sigma_{\mathrm{Au}} + \sigma_{abs\ \mathrm{Au}}(E_1)]\}, \tag{21}
$$

where ρ_f and d_f are the filter atomic density and thickness, respectively, while $\sigma_{abs\ \mathrm{Au}}(E_1)$ is the Au neutron absorption cross section.[77] The delta function represents the standard time-of-flight law on which VESUVIO is based,[54] and finally, it is worthwhile to recall that $(d^2\sigma/d\Omega\, d\omega)_{\mathrm{DINS}}$ can be cast as a function of E_0, E_1, and θ.

Following the guidelines of Eq. (17), the model DINS response functions $\langle F_n(y_n,\mathbf{Q})\rangle_\Omega$ were transformed into simulated TOF spectra $I_n(t,\langle\theta\rangle)$ (with $n=\{\mathrm{H},{}^{35}\mathrm{Cl},{}^{37}\mathrm{Cl}\}$) detector by detector, using the following relationship:

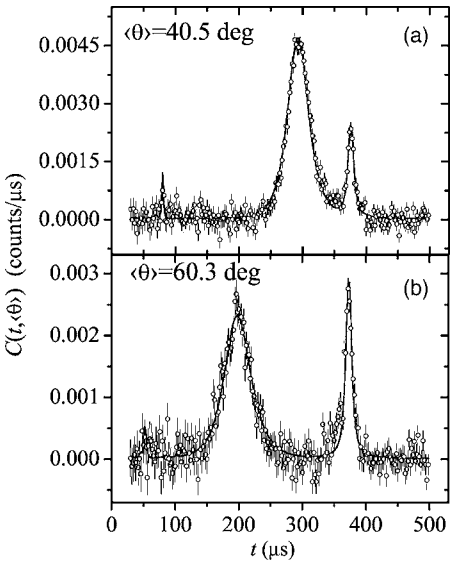

FIG. 3. Examples of fits (full line) of experimental neutron time-of-flight spectra (empty circles with error bars) at two selected $\langle\theta\rangle$ values, namely, $\langle\theta\rangle=40.5°$ (a) and $\langle\theta\rangle=60.3°$ (b). Background has been removed from both experimental data and fits. Left-side broad peak is caused by H, while right-side narrow peak by ^{35}Cl plus ^{37}Cl.

$$I_n(t,\langle\theta\rangle) = \int_{-\infty}^{\infty} dt_0 \int_0^{\pi} d\theta \int_0^{\infty} dL_0 \int_0^{\infty} dL_1 P(t_0,\theta,L_0,L_1) \times \int_0^{\infty} dE_0 \Phi(E_0) \int_0^{\infty} dE_1\, \eta(E_1) \times [1 - T_{\mathrm{Au}}(E_1)]\, \delta\left(t - t_0 - L_0 \sqrt{\frac{m_n}{2E_0}} - L_1 \sqrt{\frac{m_n}{2E_1}} \right) \frac{x_n \sigma_n}{4\pi} \sqrt{\frac{E_1}{E_0}} \frac{M_n}{\hbar^2 Q} \langle F_n(y_n,\mathbf{Q})\rangle_{\Omega}. \tag{22}$$

The previous formula was implemented via a FORTRAN code, where the neutron energy integrations were performed explicitly in the wavelength domain, while the averaging over t_0, θ, L_0, and L_1 was included through Monte Carlo routines. In this respect, we have to point out that the present calculation is an improvement of those reported in Refs. 28, 29, and 31, where the instrumental parameter uncertainties, having much less impact than the resonance peak shape $T_{\mathrm{Au}}(E_1)$, were simply disregarded. Special care was devoted to checking the numerical stability of the computed $I_n(t,\langle\theta\rangle)$.

Once having obtained all the simulated TOF spectra $I_n(t,\langle\theta\rangle)$, a linear fitting procedure was set up in order to analyze the experimental single-scattering spectra $C_1(t,\langle\theta\rangle)$:

$$C_1(t,\langle\theta\rangle) = A_{\langle\theta\rangle}[R_{\mathrm{H}}(\langle\theta\rangle) I_{\mathrm{H}}(t,\langle\theta\rangle) + I_{^{35}\mathrm{Cl}}(t,\langle\theta\rangle) + I_{^{37}\mathrm{Cl}}(t,\langle\theta\rangle)] + B_{\langle\theta\rangle}(t), \tag{23}$$

where $A_{\langle\theta\rangle}$ is an overall detector-dependent scaling constant, $R_{\mathrm{H}}(\langle\theta\rangle)$ is the *anomalous reduction factor for the proton cross section*, and $B_{\langle\theta\rangle}(t)$ is a detector-dependent polynomial background of the second order in t, making a total of five independent parameters per spectrum. The actual fitting procedure was implemented through a FORTRAN code making use of the MINUIT standard minimizing routine.[78] Experimental data were fitted in the TOF interval $30<t<498$ μs. Examples of the quality of the present fits are reported in Figs. 3(a) and 3(b) for detectors placed at two selected $\langle\theta\rangle$ values. The agreement between experimental and simulated data is very good in the whole TOF interval since reduced χ^2 never exceeds 1.27 for all the spectra, exhibiting an average value of 1.07 ± 0.10. However, such an agreement could be reached only by progressively reducing the value of $R_{\mathrm{H}}(\langle\theta\rangle)$, as $\langle\theta\rangle$ grew, with respect to the figure established by the standard neutron scattering theory: $R_{\mathrm{H}}(\langle\theta\rangle)=1$. To be more exact, one should expect $R_{\mathrm{H}}(\langle\theta\rangle)=1.00\pm0.03$, due to the uncertainties[17] on the σ_n values used in Eq. (22). The best-fit estimates of $R_{\mathrm{H}}(\langle\theta\rangle)$ are reported in Fig. 4 where discrepancies from the expected value are clearly visible.

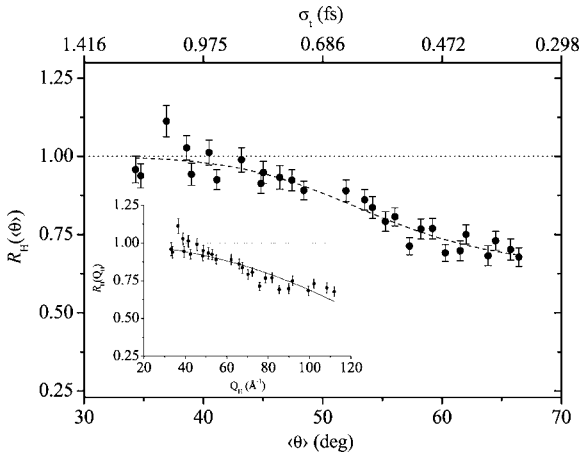

FIG. 4. Experimental estimates of the anomalous reduction factor for the proton cross section $R_{\mathrm{H}}(\langle\theta\rangle)$ (full circles with error bars) together with a heuristic fit of its angular behaviour (dashed line). Dotted line marks the standard neutron scattering theory prediction [i.e., $R_{\mathrm{H}}(\langle\theta\rangle)=1$]. Upper abscissa reports the typical time-window values of the scattering event, σ_t. The inset shows the corresponding $R_{\mathrm{H}}(Q_{\mathrm{H}})$ (full circles with error bars), together with the Q_{H}-dependent model fit of Eq. (26) (continuous line). Dotted line marks the standard neutron scattering theory prediction.

V. DISCUSSION

The fitting results from the experimental DINS spectra, plotted in Fig. 4, clearly show that the neutron scattering cross-section of protons in orthorhombic ordered HCl undergoes an anomalous reduction in the VESUVIO measurements moving from a scattering angle of about 33° to roughly 65°. In order to better estimate such a reduction, a heuristic fit of $R_{\mathrm{H}}(\langle\theta\rangle)$ has been performed using a Boltzmann-type function:

$$R_{\mathrm{H}}^{(f)}(\langle\theta\rangle) = \frac{1-R_{\infty}}{1+\exp[(\langle\theta\rangle-\theta_{sw})d\theta^{-1}]} + R_{\infty}, \tag{24}$$

where R_{∞} is the high-angle asymptotic value of the reduction factor, θ_{sw} is the "switching" angle, and $d\theta$ controls the

steepness of the reduction. The following parameter values have been obtained: $R_\infty = 0.66 \pm 0.03$, $\theta_{sw} = (53 \pm 1)°$, and $d\theta = (5.1 \pm 0.9)°$, indicating that a 34% reduction of σ_H occurs, centered around $\langle\theta\rangle \simeq 53°$ with a typical width of about 5°. In order to gain a more physical insight about this phenomenon, it is convenient to approximately transform TOF and scattering angles into wave-vector and energy transfers, fixing $E_1 = E_r$. Under this coarse assumption and dealing with the centroid of the H recoil peak (labeled Q_H and $\hbar\omega_H$), one writes

$$Q_H = \sqrt{\frac{2m_n E_r}{\hbar^2}} \tan\theta,$$

$$\hbar\omega_H = \frac{\hbar^2 Q_H^2}{2M_H}, \tag{25}$$

which imply that the present DINS experiment explores the following proton dynamical range: $31.6 < Q_H < 104$ Å^{-1} and $2070 < \hbar\omega_H < 22600$ meV, showing a "switch" at $Q_H \simeq 64.6$ Å^{-1} and $\hbar\omega_H \simeq 8640$ meV on a typical scale of $\Delta Q_H \simeq 11.9$ Å^{-1} and $\Delta\hbar\omega_H \simeq 3260$ meV. The inset of Fig. 4 reports the corresponding $R_H(Q_H)$ showing the Q_H dependence of the reduction factor. Recent theories[79] indicate that a breakdown of the Born-Oppenheimer approximation in the final state of the scattering process, where nonadiabatic electronic excitations are probed, would be responsible for the reduction factor. In these theories $R_H(Q_H) \propto Q_H^2$, and in the inset of Fig. 4 a fit of the form

$$R_H(Q_H) = a + bQ_H^2 \tag{26}$$

is also reported. The corresponding best-fitting parameter values have been obtained: $a = 0.99 \pm 0.01$, $b = (-3.0 \times 10^{-5} \pm 3.0 \times 10^{-6})$ Å^2. The comparison among the heuristic and parabolic model fitting functions results in a compatibility of both model functions with the experimental reduction factor. In order to better test the accuracy of the models, we envisage that measurements in a more extended Q_H range, for example employing higher energy neutron absorption analyzers, would explore regions where clear saturation effects may be observed.

In addition, given the frequency width of the H recoil peak, $\langle(\omega - \langle\omega\rangle)^2\rangle$ (once expressed as self inelastic structure factor), namely,[19]

$$\langle(\omega - \langle\omega\rangle)^2\rangle = \frac{2\langle E_K\rangle Q^2}{3M_H}, \tag{27}$$

with $\langle E_K\rangle$ being the single H mean kinetic energy, it is possible to evaluate the time scale σ_t of the DINS scattering process through the well-known Fourier transform relationship: $\sigma_t^2 = \langle(\omega - \langle\omega\rangle)^2\rangle^{-1}$. In the framework of the impulsive approximation and making use of the West scaling variable introduced in Eq. (3) it is moreover straightforward to relate the time window to the momentum transfer in the scattering process. Thus one observes in Fig. 4 that the relevant time windows of the experiment lie in the sub femtosecond domain: $1.26 \times 10^{-15} < \sigma_t < 3.83 \times 10^{-16}$ s, with a "switching" time window of 6.16×10^{-16} s, not far from the figure extracted in a previous eVS experimental work on niobium hydride[18] [i.e., $4-5 \times 10^{-16}$ s].

The comparison with earlier studies on the anomalous reduction of the DINS proton cross-section poses an important data-analysis question about the reliability of the published results. As pointed out in Sec. I, the codes routinely used to extract the experimental values of the DINS proton cross section[80] (namely TFIT or TFIT-FSE) have been heavily criticized in Refs. 28, 29, and 31, while Ref. 32, on the contrary, showed that TFIT or TFIT-FSE provided results in good agreement with a full Monte Carlo simulation of the VESUVIO spectrometer. In addition, in parallel to comparison with Monte Carlo simulations, careful experimental tests of the uncertainties related to the spectrometer components, including the energy-dependent incident beam intensity, calibration of primary and secondary flight paths, sample geometry effects, multiple scattering and attenuation effects, detector dead time and saturation effects, have been carried out recently,[32,81,82] ruling out any influence on the observed anomaly. What has never been attempted is to compare the data analysis approach outlined in Refs. 28, 29, and 31 with the standard VESUVIO data analysis approach which raised the main criticisms to the results of proton cross-section measurements. Now it is finally possible to solve this paradox, since phase-III HCl data, already analyzed in Sec. IV following the prescriptions of Refs. 28, 29, and 31, can be easily re-processed, this time through TFIT-FSE (more advanced than TFIT). Before presenting the new $R_H(\langle\theta\rangle)$ determinations from TFIT-FSE, it is worth spending a few words on the TFIT-FSE code itself. Making use of the symbols introduced in Secs. III and IV, one can condense the basic assumptions of this fitting routine in the formula:

$$C_1(t,\langle\theta\rangle) \simeq K \int_0^\infty dE_0 \Phi(E_0) \delta\left(t - \langle t_0\rangle - \langle L_0\rangle \sqrt{\frac{m_n}{2E_0}} - \langle L_1\rangle \sqrt{\frac{m_n}{2E_r}}\right) \left(\frac{d^2\sigma}{d\Omega\, d\hbar\omega}\right)_{\mathrm{DINS}}, \tag{28}$$

where K is an appropriate instrumental constant, and $(d^2\sigma/d\Omega\, d\hbar\omega)_{\mathrm{DINS}}$ is cast in the following approximate form to include the VESUVIO resolution effects through the so-called convolution approximation:

$$\left(\frac{d^2\sigma}{d\Omega\, d\hbar\omega}\right)_{\mathrm{DINS}} \simeq \sqrt{\frac{E_r}{E_0}} \sum_n x_n \frac{\sigma_n}{4\pi} \frac{M_n}{\hbar^2 Q} F_n(y_n, Q) \otimes V_n(y_n), \tag{29}$$

with $V_n(y_n)$ being a mass-dependent Voigt function determined through the instrument calibration procedure.[83] As for the response functions chosen by TFIT-FSE, no spherical average of anisotropic profiles is accomplished, but the following standard isotropic expression[58] is used:

$$F_n(y_n, Q) \simeq \left(1 + \frac{A_3^{(n)}(Q)}{(2\sigma_{p,n}^2)^{3/2}} H_3[y_n(2\sigma_{p,n}^2)^{-1/2}]\right) \frac{1}{\sqrt{2\pi}\sigma_{p,n}} \times \exp\left(-\frac{y_n^2}{2\sigma_{p,n}^2}\right), \tag{30}$$

where the standard deviations $\sigma_{p,n}$ are fitting parameters,

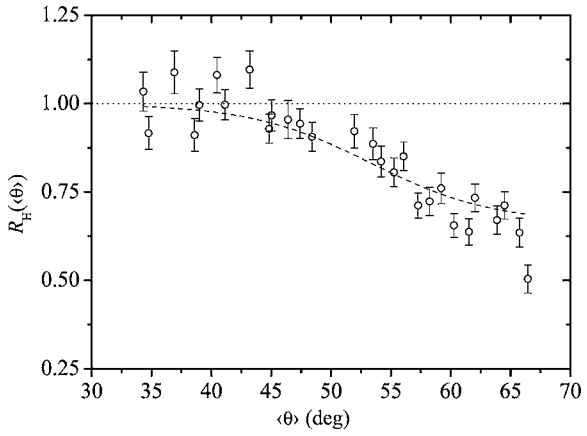

FIG. 5. Experimental estimates of the anomalous reduction factor for the proton cross section $R_H(\langle\theta\rangle)$ (empty circles with error bars) derived from the TFIT-FSE code, together with the results reported in Fig. 4 (dashed line). Dotted line marks the standard neutron scattering theory prediction [i.e., $R_H(\langle\theta\rangle)=1$].

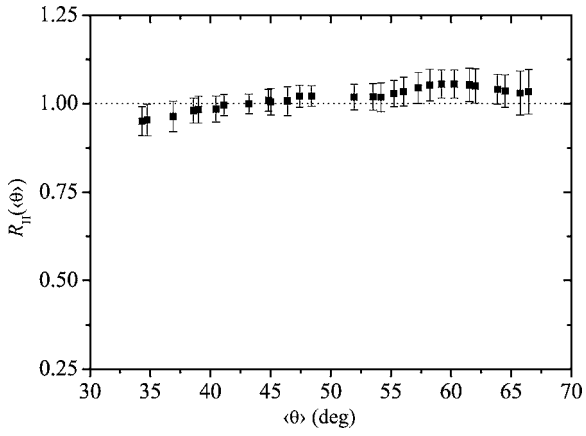

FIG. 6. Simulated data analysis: estimates of the anomalous reduction factor for the proton cross section $R_H(\langle\theta\rangle)$ (full squares with error bars) derived from the TFIT-FSE code used on data simulated through Eq. (17). Dotted line marks the expected value $R_H(\langle\theta\rangle)=1$.

while $A_3^{(n)}(Q)$ are approximated as in a three-dimensional isotropic harmonic oscillator (at $T=0$) by $A_3^{(n)}(Q)=\sigma_{p,n}^4/(3Q)$. The older version of the code, namely, TFIT, did not include the FSE correction term $A_3^{(n)}(Q)=0$.

Experimental VESUVIO data $C_1(t,\langle\theta\rangle)$ are fitted by TFIT-FSE in the TOF interval $30<t<498$ μs making use of an overall scaling constant, an anomalous reduction factor, two $\sigma_{p,n}$ values (for $n=\{H,Cl\}$), and a parabolic background (a total of seven parameters), similarly to Eq. (23). The agreement between experimental and fitted data is good in the whole TOF interval (average reduced $\chi^2=1.04\pm0.11$), comparable with the quality of the Eq. (22) approach. The TFIT-FSE estimates of $R_H(\langle\theta\rangle)$ are reported in Fig. 5 where deviations from $R_H(\langle\theta\rangle)=1$ are evident. Moreover, comparing the heuristic Boltzmann-type curve from Fig. 4 to the present TFIT-FSE estimates, it is possible to observe that, despite a rather larger scattering of the TFIT-FSE data points, the two approaches provide basically the same answer to the problem of the anomalous reduction of the DINS proton cross-sections. We stress however that the use of the standard isotropic expression of Eq. (30) with $\sigma_{p,n}$ as fitting parameters results in an underestimation of $\sigma_{p,H}$ and, consequently, of the single H mean kinetic energy, $\langle E_K\rangle_H=3\hbar^2\sigma_{p,H}^2/2M_H$. A simple Gaussian model, although being adequate to capture the essential features of the anomalous reduction factor, is not adequate to finely describe the experimental response function with regards to the second and higher spectral moments. In particular, the derived value of $\langle E_K\rangle_H$ using TFIT-FSE is 66 ± 1 meV to be compared with a value of 98.996 meV obtained from the model anisotropic response function. Such discrepancies can be argued by comparing the spherically averaged response function and the simple Gaussian response function reported in Fig. 1. This finding, as already pointed out in the case of DINS studies on H_2S (Ref. 12) and H_2O (Ref. 11) by the eVS-VESUVIO spectrometers, confirms that appropriate response models beyond simple Gaussian line shapes are needed in order to analyze DINS experimental response functions $\langle J_H(y_H,\hat{\mathbf{Q}})\rangle_\Omega$ in hydrogen-containing diatomic and polyatomic molecules.

A more complete understanding of the errors introduced by the approximations in TFIT-FSE for the determination of anomalous reduction factors can be simply obtained by using this code in conjunction with TOF spectra simulated through Eq. (17). Choosing the same values of the VESUVIO instrumental parameters $\langle t_0\rangle$, $\langle\theta\rangle$, $\langle L_0\rangle$, and $\langle L_1\rangle$ and the accepted neutron cross-section values σ_n,[17] various $C_1(t,\langle\theta\rangle)$ have been generated and, after the addition of appropriate Poisson noise to simulate a realistic statistical accuracy, they were fitted via TFIT-FSE in the TOF interval $30<t<498$ μs. This four-parameter fit [an overall scaling constant, an anomalous reduction factor and two $\sigma_{p,n}$ values (for $n=\{H,Cl\}$)] provided estimates of $R_H(\langle\theta\rangle)$, plotted in Fig. 6. As is evident, the deviations from unity, which exhibit an angular trend opposite to those in Figs. 4 and 5, never exceed the 5.6% limit in all the TOF range, with a root mean squared value of 3.4%. This figure has to be compared with the anomalous reduction estimated from the experimental VESUVIO data (namely, $34\pm3\%$), which is about ten times larger, proving not only the effectiveness of the present evaluation of $R_H(\langle\theta\rangle)$, but, moreover, the essential reliability of all the previous work done on the anomalous DINS proton cross-sections (see for example Refs. 16, 18, and 20–25), at least within an accuracy level of 5–6 %. Again, the use of the simple Gaussian isotropic proton response function appears adequate for the determination of $R_H(\langle\theta\rangle)$, although at the expenses of an accurate determination of the one-dimensional momentum distribution. We therefore conclude that such a cross-section reduction is a novel and genuine condensed-matter phenomenon, for which no final explanation still exists, despite a number of interesting,[84,85,79] but rather controversial,[86] hypotheses.

VI. CONCLUSIONS

In the present paper deep inelastic neutron scattering measurements from orthorhombic ordered HCl have been pre-

sented and carefully analyzed in order to clarify the puzzling problem of the anomalous deficit in the neutron-proton cross section at energy transfer values in the 2–20 eV range. Such an analysis has been performed in three distinct phases. (1) We set up a reliable model for the HCl short-time single-particle dynamics, which could capture its most important features, namely the anisotropy of the atomic vibrational environment and the deviations from the impulsive approximation due to the relative strength of the crystal force constants. This task has been accomplished in detail making use of lattice dynamics calculations and with the inclusion of no adjustable parameter. (2) We transform the HCl response function calculated at point (1) into simulated time-of-flight spectra in the most rigorous way, taking into account all the criticisms raised in Refs. 28, 29, and 31 concerning the effects of instrumental resolution and filter absorption profile. (3) We compare processed VESUVIO data (indeed corrected for multiple scattering and self-absorption) with simulated time-of-flight spectra from point (2), in order to extract the experimental values of proton and chlorine cross sections (bound) and, from these, the anomalous reduction factor for the former.

Results pointed out the existence of a 34% reduction of the proton-neutron cross section, varying with the scattering angle in a 10° interval centered at 53°, similarly to previous findings on niobium hydride. Moreover, the same approximate procedure used in the earlier studies on this subject (actually implemented via TFIT or TFIT-FSE codes[80]) was employed to reanalyze the present HCl data, and provided results in agreement with those from the more rigorous treatment, as far as the anomalous reduction factor is concerned. Thus it was concluded that, confirming the findings of Ref. 32, all the past DINS work on the anomalous deficit of the proton-neutron cross section appears basically sound and reliable, at least within an accuracy level of 5–6 %, which then represents the typical size of the errors induced by the approximations criticized in Refs. 28, 29, and 31. The complete explanation of these results remains a challenge to conventional condensed matter theories.

ACKNOWLEDGMENTS

We acknowledge the financial support of the Consiglio Nazionale delle Ricerche (CNR)-Italy within the CNR-CCLRC agreement. The authors thank the ISIS User Support Group for the excellent technical help provided, in addition pleasant and stimulating discussions with Professor C. Andreani and Dr. M. Zoppi on the subject of this paper are gratefully acknowledged. Finally, Dr. J. D. Gale (Imperial College, London, UK) is warmly thanked for kindly providing one of the authors (D.C.) with his GULP code.

*Corresponding author. FAX: +39-06-2023507. Email address: roberto.senesi@roma2.infn.it

[1] G. I. Watson, J. Phys.: Condens. Matter **8**, 5955 (1996).
[2] R. A. Cowley and A. D. B. Woods, Phys. Rev. Lett. **21**, 787 (1968).
[3] O. K. Harling, Phys. Rev. Lett. **24**, 1046 (1970).
[4] H. A. Mook, Phys. Rev. Lett. **32**, 1167 (1974).
[5] V. F. Sears, E. C. Svensson, P. Martel, and A. D. B. Woods, Phys. Rev. Lett. **49**, 279 (1982).
[6] K. W. Herwig, P. E. Sokol, T. R. Sosnick, W. M. Snow, and R. C. Blasdell, Phys. Rev. B **41**, 103 (1990); H. R. Glyde, R. T. Azuah, and W. G. Stirling, *ibid.* **62**, 14337 (2000).
[7] R. O. Hilleke, P. Chaddah, R. O. Simmons, D. L. Price, and S. K. Sinha, Phys. Rev. Lett. **52**, 847 (1984); S. O. Diallo, J. V. Pearce, R. T. Azuah, and H. R. Glyde, *ibid.* **93**, 075301 (2004).
[8] D. A. Peek, M. C. Schmidt, I. Fujita, and R. O. Simmons, Phys. Rev. B **45**, 9671 (1992); R. T. Azuah, W. G. Stirling, H. R. Glyde, P. E. Sokol, and S. M. Bennington, *ibid.* **51**, 605 (1995).
[9] J. Mayers, Phys. Rev. Lett. **71**, 1553 (1993); U. Bafile, M. Celli, M. Zoppi, and J. Mayers, Phys. Rev. B **58**, 791 (1998); C. Andreani, D. Colognesi, and E. Pace, *ibid.* **60**, 10008 (1999).
[10] A. L. Fielding, D. N. Timms, and J. Mayers, Europhys. Lett. **44**, 255 (1998).
[11] C. H. Uffindell, A. I. Kolesnikov, J.-C. Li, and J. Mayers, Phys. Rev. B **62**, 5492 (2000); C. Andreani, D. Colognesi, E. Degiorgi, and M. A. Ricci, J. Chem. Phys. **115**, 43 (2001).
[12] C. Andreani, E. Degiorgi, R. Senesi, F. Cilloco, D. Colognesi, J. Mayers, M. Nardone, and E. Pace, J. Chem. Phys. **114**, 387 (2001).
[13] A. C. Evans, D. N. Timms, J. Mayers, and S. M. Bennington, Phys. Rev. B **53**, 3023 (1996).
[14] D. Colognesi, A. J. Ramirez-Cuesta, M. Zoppi, R. Senesi, and T. Abdul-Redah, Physica B **350**, e983 (2004).
[15] G. F. Reiter, J. Mayers, and P. Platzman, Phys. Rev. Lett. **89**, 135505 (2002).
[16] C. A. Chatzidimitriou-Dreismann, T. A. Redah, R. M. F. Streffer, and J. Mayers, Phys. Rev. Lett. **79**, 2839 (1997).
[17] V. F. Sears, Neutron News **3**, 26 (1992).
[18] E. B. Karlsson, C. A. Chatzidimitriou-Dreismann, T. Abdul-Redah, R. M. F. Streffer, B. Hjörvarsson, J. Öhrmalm, and J. Mayers, Europhys. Lett. **46**, 617 (1999).
[19] S. W. Lovesey, *Theory of Neutron Scattering from Condensed Matter* (Clarendon Press, Oxford, 1984).
[20] C. A. Chatzidimitriou-Dreismann, T. Abdul-Redah, R. M. F. Streffer, and J. Mayers, J. Chem. Phys. **116**, 1511 (2002).
[21] C. A. Chatzidimitriou-Dreismann, T. Abdul-Redah, and J. Sperling, J. Chem. Phys. **113**, 2784 (2000).
[22] C. A. Chatzidimitriou-Dreismann, M. Vos, C. Kleiner, and T. Abdul-Redah, Phys. Rev. Lett. **91**, 057403 (2003); M. Vos, C. A. Chatzidimitriou-Dreismann, T. Abdul-Redah, and J. Mayers, Nucl. Instrum. Methods Phys. Res. B **227**, 233 (2004).
[23] E. B. Karlsson, T. Abdul-Redah, R. M. F. Streffer, B. Hjörvarsson, J. Mayers, and C. A. Chatzidimitriou-Dreismann, Phys. Rev. B **67**, 184108 (2003).
[24] C. A. Chatzidimitriou-Dreismann and T. Abdul-Redah, Physica B **350**, 239 (2004).
[25] T. Abdul-Redah and C. A. Chatzidimitriou-Dreismann, Physica B **350**, E1035 (2004).

[26] A. C. Evans, J. Mayers, D. N. Timms, and M. J. Cooper, Z. Naturforsch., A: Phys. Sci. **48**, 425 (1993).
[27] R. Senesi, C. Andreani, Z. Bowden, D. Colognesi, E. Degiorgi, A. L. Fielding, J. Mayers, M. Nardone, J. Norris, M. Praitano, N. J. Rhodes, W. G. Stirling, J. Tomkinson, and C. Uden, Physica B **276–278**, 200 (2000); J. Mayers, J. Tomkinson, T. Abdul-Redah, W. G. Stirling, C. Andreani, R. Senesi, M. Nardone, D. Colognesi, E. Degiorgi, *ibid.* **350**, E659 (2004).
[28] J. J. Blostein, J. Dawidowski, and J. R. Granada, Physica B **304**, 357 (2001).
[29] J. J. Blostein, J. Dawidowski, and J. R. Granada, Nucl. Instrum. Methods Phys. Res. B **217**, 333 (2004); J. J. Blostein, J. Dawidowski, and J. R. Granada, Phys. Rev. B **71**, 054105 (2005).
[30] R. A. Cowley, J. Phys.: Condens. Matter **15**, 4143 (2003).
[31] J. J. Blostein, J. Dawidowski, and J. R. Granada, Physica B **334**, 257 (2003).
[32] J. Mayers and T. Abdul-Redah, J. Phys.: Condens. Matter **16**, 4811 (2004).
[33] A. Ioffe, M. Arif, D. L. Jacobson, and F. Mezei, Phys. Rev. Lett. **82**, 2322 (1999).
[34] J. J. Blostein, J. Dawidowski, S. A. Ibáñez, and J. R. Granada, Phys. Rev. Lett. **90**, 105302 (2003).
[35] C. A. Chatzidimitriou-Dreismann, U. K. Krieger, A. Möller, and M. Stern, Phys. Rev. Lett. **75**, 3008 (1995).
[36] C. Halcoussis, T. Abdul-Redah, H. Naumann, G. Monaco, and C. A. Chatzidimitriou-Dreismann, ESRF Newsletter **34**, 17 (2000).
[37] E. Sàndor and R. F. C. Farrow, Nature (London) **213**, 171 (1967).
[38] K. P. Huber and G. Herzberg, *Molecular Spectra and Molecular Structure* (Van Nostrand Reinhold, New York, 1979), Vol. IV.
[39] C. H. Wang, and P. A. Fleury, J. Chem. Phys. **53**, 2243 (1970); A. Anderson, B. H. Torrie, and W. S. Tse, J. Raman Spectrosc. **10**, 148 (1981).
[40] G. L. Hiebert, and D. F. Hornig, J. Chem. Phys. **27**, 1216 (1957); A. Anderson, H. A. Gebbie, and S. H. Walmsley, Mol. Phys. **7**, 401 (1964).
[41] H. Boutin and S. Yip, *Molecular Spectroscopy with Neutrons* (MIT Press, Cambridge, MA, 1968).
[42] D. Colognesi, C. Andreani, and E. Degiorgi, J. Neutron Res. **11**, 123 (2003).
[43] P. J. Grout and J. W. Leech, J. Phys. C **7**, 3245 (1974).
[44] N. S. Gillis, J. C. Raich, L. B. Kanney, and A. Bickermann, J. Chem. Phys. **64**, 2501 (1976).
[45] J. F. Higgs, W. Y. Zeng, and A. Anderson, Phys. Status Solidi B **133**, 475 (1986).
[46] C.-N. Chang, W.-S. Tse, and C. Li, Chin. J. Phys. (Taipei) **21**, 11 (1983).
[47] K. T. No and M. S. Jhon, Bull. Korean Chem. Soc. **6**, 183 (1985).
[48] V. Schettino and P. R. Salvi, Chem. Phys. **41**, 439 (1979).
[49] E. Katoh, H. Yamawaki, H. Fujihisa, M. Sakashita, and K. Aoki, Phys. Rev. B **61**, 119 (2000), and references therein.
[50] N. Niimura, K. Shimaoka, H. Motegi, S. Hoshino, J. Phys. Soc. Jpn. **32**, 1019 (1972).
[51] N. G. Parsonage and L. A. K. Staveley, *Disorder in Crystals* (Clarendon Press, Oxford, 1978).
[52] C. Andreani, M. A. Ricci, M. Nardone, F. P. Ricci, and A. K. Soper, J. Chem. Phys. **107**, 214 (1997).
[53] P. A. Seeger, A. D. Taylor, and R. M. Brugger, Nucl. Instrum. Methods Phys. Res. A **240**, 98 (1985).
[54] C. G. Windsor, *Pulsed Neutron Scattering* (Taylor and Francis, London, 1981).
[55] S. F. Mughabghab, M. Divadeenam, N. E. Holden, *Neutron Cross-Sections* (Academic Press, New York, 1981), Vol. I.
[56] D. R. Stull, Ind. Eng. Chem. **39**, 517 (1947).
[57] V. F. Turchin, *Slow Neutrons* (Israel Program for Scienfic Translations, Jerusalem, 1967).
[58] V. F. Sears, Phys. Rev. B **30**, 44 (1984).
[59] H. R. Glyde, Phys. Rev. B **50**, 6726 (1994).
[60] V. F. Sears, Phys. Rev. **185**, 200 (1969).
[61] A. S. Rinat, Phys. Rev. B **36**, 5171 (1987).
[62] H. A. Gersch, L. J. Rodriguez, and P. N. Smith, Phys. Rev. A **5**, 1547 (1972); H. A. Gersch and L. J. Rodriguez, *ibid.* **8**, 905 (1973).
[63] A. Rahman, K. S. Singwi, and A. Sjölander, Phys. Rev. **126**, 986 (1962).
[64] G. Corradi, D. Colognesi, M. Celli, and M. Zoppi, Condens. Matter Phys. **6**, 499 (2003).
[65] V. F. Sears, Can. J. Phys. **63**, 68 (1985).
[66] K. S. Singwi and M. P. Tosi, Phys. Rev. **149**, 70 (1966).
[67] J. M. F. Gunn and M. Warner, Z. Phys. B: Condens. Matter **56**, 13 (1984).
[68] D. Colognesi, M. Celli, and M. Zoppi, J. Chem. Phys. **120**, 5657 (2004).
[69] J. Boronat, C. Cazorla, D. Colognesi, and M. Zoppi, Phys. Rev. B **69**, 174302 (2004).
[70] A. I. Kolesnikov and J.-C. Li, Physica B **234–236**, 34 (1997).
[71] J. D. Gale, Philos. Mag. B **73**, 3 (1996); J. Chem. Soc., Faraday Trans. **93**, 629 (1997).
[72] Yu. A. Izyumov and N. A. Chernoplekov, *Neutron Spectroscopy* (Consultants Bureau, New York, 1994).
[73] H. J. Monkhorst and J. D. Pack, Phys. Rev. B **13**, 5188 (1972).
[74] W. R. Shields, T. J. Murphy, E. L. Garner, and V. H. Dibeler, J. Am. Chem. Soc. **84**, 1519 (1962).
[75] H. H. Paalman and C. J. Pings, J. Appl. Phys. **33**, 2635 (1962).
[76] J. Mayers, A. L. Fielding, and R. Senesi, Nucl. Instrum. Methods Phys. Res. A **481**, 454 (2002).
[77] V. McLane, C. L. Dunford, and P. F. Rose, *Neutron Cross Sections* (Academic Press, San Diego, 1988), Vol. II.
[78] F. James, *MINUIT Minimization Package: Reference Manual* (CERN Program Library, Geneva, 1994).
[79] N. I. Gidopoulos, Phys. Rev. B **71**, 054106 (2005); G. F. Reiter and P. M. Platzman, *ibid.* **71**, 054107 (2005).
[80] J. Mayers, Rutherford Appleton Laboratory Technical Report No. RAL-TR-96-067, 1996 (unpublished).
[81] A. L. Fielding and J. Mayers, Nucl. Instrum. Methods Phys. Res. A **480**, 680 (2002).
[82] C. A. Chatzidimitriou-Dreismann, T. Abdul-Redah, and J. Mayers, Physica B **315**, 281 (2002).
[83] J. Mayers and A. C. Evans, Rutherford Appleton Laboratory Technical Report No. RAL-91-048, 1991 (unpublished).
[84] E. B. Karlsson and S. W. Lovesey, Phys. Rev. A **61**, 062714 (2000); Phys. Scr. **65**, 112 (2002); E. B. Karlsson, Phys. Rev. Lett. **90**, 095301 (2003).
[85] C. A. Chatzidimitriou-Dreismann, J. Alloys Compd. **356–357**, 244 (2003).
[86] R. A. Cowley, J. Phys.: Condens. Matter **15**, 4143 (2003); D. Colognesi, Physica B **344**, 73 (2003); **358**, 114 (2005).